^{18}F-FDG PET based intratumoral and peritumoral explainable radiomics for predicting cervical cancer prognosis: A multi-center retrospective study

Ruihe Lai[1] **MD,**
Dandan Sheng[2] **Bsc,**
Yuzhi Geng[2] **Msc,**
Chongyang Ding[3*] **MD,**
Tingting Tang[4*]
Zhengyang Zhou[5*] **MD**

**Zhengyang Zhou, Tingting Tang and Chongyang Ding are co-corresponding authors*

1. Department of Nuclear Medicine, Nanjing Drum Tower Hospital, Clinical College of Nanjing Medical University, Nanjing, China
2. Department of Nuclear Medicine, The Second Affiliated Hospital of Nanjing Medical University, Nanjing, China
3. Department of Nuclear Medicine, The First Affiliated Hospital of Nanjing Medical University, Nanjing, China
4. Department of Obstetrics and Gynecology, Nanjing Drum Tower Hospital, Clinical College of Nanjing Medical University, Nanjing, China.
5. Department of Radiology, Nanjing Drum Tower Hospital Clinical College of Nanjing Medical University, Nanjing, China.

Keywords: ^{18}F-FDG PET - Radiomics - Peritumoral - Cervical cancer - Prognosis - Shapley additive explanations

Corresponding author:
Zhengyang Zhou
Department of Radiology, Nanjing Drum Tower Hospital, Clinical College of Nanjing Medical University, Nanjing, China
zyzhou@nju.edu.cn
Tel:+86-18795840983
Tingting Tang
Department of Obstetrics and Gynecology,
Nanjing Drum Tower Hospital, Clinical College of Nanjing Medical University, Nanjing, China
Tel:+86-18845130337
18260062993@163.com
Chongyang Ding
Department of Nuclear Medicine, The First Affiliated Hospital of Nanjing Medical University, Nanjing, China
Tel:+15951614327
chongyangding@163.com

Received:
14 October 2025
Accepted revised:
8 December 2025

Abstract

Objective: Prognosis evaluation in cervical cancer is crucial for treatment decisions. This study aims to develop and validate a combined model using positron emission tomography (PET)-derived intratumoral and peritumoral radiomic parameters to predict cervical cancer prognosis based on the Shapley additive explanations (SHAP) method. **Subjects and Methods:** A retrospective cohort of 114 patients with cervical cancer from two institutions was used, with one institution's data designated for training and the other for testing. Semi-automatic segmentation of fluorine-18-fluorodeoxyglucose (^{18}F-FDG) PET images was performed to delineate the primary intratumoral and peritumoral regions, defined by expanding the tumor boundary by 2mm, 4mm, 6mm, and 8mm. Radiomic features were extracted from each region. Six machine learning algorithms were employed to construct intratumoral and peritumoral radiomic models, with the optimal model selected based on performance evaluated through receiver operating characteristic (ROC) and calibration curves. Area under the curve (AUC) values were compared using the DeLong test. The SHAP method was used to identify the key features influencing prognosis. **Results:** Among the intratumoral and peritumoral radiomic models, the Gradient Boosting Machine (GBM) algorithm showed superior performance. The 4mm peritumoral model exhibited the best performance among the four peritumoral models, with a testing AUC of 0.762 (95% CI: 0.582-0.944). The integrated model combining the intratumoral and 4mm peritumoral regions emerged as the optimal radiomic model for predicting cervical cancer prognosis, achieving the highest AUC of 0.954 (95% CI: 0.882-1.000) in the testing set. At the patient level, SHAP force plots provided valuable insights into the combined model's predictive ability for prognosis. **Conclusion:** The integrated radiomic model, particularly for the 4mm peritumoral region, was validated as the optimal approach for predicting overall survival in cervical cancer. The application of the SHAP method enhanced interpretability, allowing for the identification of key features influencing prognosis and offering transparent insights for guiding personalized treatment strategies.

Hell J Nucl Med 2025; 28(3): 246-255 *Epub ahead of print: 15 December 2025* *Published online: 30 December 2025*

Introduction

Cervical cancer ranks as the fourth most common malignancy among women, with an estimated 0.66 million new cases and 0.35 million deaths worldwide in 2022 [1]. The prognosis of cervical cancer is influenced by several factors, including lymph node status, the International Federation of Gynecology and Obstetrics (FIGO) staging, histological type, and tumor size [2]. According to international guidelines [3], surgery is the preferred treatment for patients with FIGO stage IA to IIA cervical cancer, while cisplatin-based chemotherapy combined with radiation therapy is the treatment of choice for those with locally advanced disease. Despite these interventions, approximately one-third of patients experience recurrence within two years of chemoradiotherapy, resulting in a 5-year overall survival rate of approximately 70% [4]. These challenges highlight the pressing need for a reliable, non-invasive method to preoperatively predict the prognosis of patients with cervical cancer, facilitating personalized treatment strategies, improving patient outcomes, and reducing recurrence.

In recent years, radiomics has emerged as a powerful research tool that not only extracts features such as tumor morphology, texture, and density but also uncovers changes in the tumor microenvironment. Specifically, features derived from both the tumor's internal and external regions through fluorine-18-fluorodeoxyglucose (^{18}F-FDG) positron emission tomography (PET) imaging offer deeper insights into tumor biology [5-8]. However, most existing radiomics studies primarily focus on tumor features alone, often overlooking the prognostic potential of the surrounding tumor microenvironment [9-11]. Fur-

thermore, despite the remarkable predictive capabilities of machine learning algorithms in medical image analysis, their "black box" nature complicates model interpretability, limiting clinical applicability [12]. Thus, integrating radiomic features from both the tumor and surrounding regions to develop a comprehensive prognostic model can provide a more holistic evaluation of patient prognosis, laying the foundation for personalized treatment.

This study aims to develop a comprehensive predictive model using PET-derived radiomic features from both the tumor's internal and surrounding regions to predict the prognosis of patients with cervical cancer. Radiomic features were extracted from the tumor's internal region and from surrounding areas at distances of 2mm, 4mm, 6mm, and 8mm. Four machine learning algorithms-random forest (RF), support vector machine (SVM), gradient boosting machine (GBM), and multilayer perceptron (MLP)-were utilized to construct the predictive models. The optimal machine learning algorithm and the most effective tumor-surrounding model were then selected to create an integrated radiomics model. The Shapley additive explanations (SHAP) method was applied to analyze feature importance, thereby enhancing the model's interpretability.

Subjects and Methods

Study population

This retrospective study analyzed data from 357 patients with cervical cancer diagnosed according to World Health Organization (WHO) criteria. All participants underwent ^{18}F-FDG PET/computed tomography (CT) imaging within two weeks before treatment initiation. Data were sourced from two hospitals, with inclusion and exclusion criteria detailed in Figure 1. A total of 83 cases from Nanjing Drum Tower Hospital and 31 cases from Jiangsu Provincial People's Hospital were included in the training and testing cohorts. Ethical approval was granted by the institution's ethics committee, and written informed consent was waived in accordance with relevant regulations (approval number: 2023-266-02). All procedures involving human participants adhered to the principles outlined in the 1964 Declaration of Helsinki and its subsequent amendments.

^{18}F-FDG PET/CT image acquisition

Two scanners (Veros and GEMINI GX, Philips, Amsterdam, Netherlands) were used in this study, with both institutions employing these two devices. Prior to imaging, all patients fasted for at least 6 hours and had blood glucose levels maintained below 11.1mmol/L. Each patient received an intravenous injection of 3.7MBq/kg (0.1mCi/kg) of ^{18}F-FDG. After the injection, patients rested in a dimly lit, quiet environ-ment for approximately 60 minutes before the scan and were instructed to empty their bladders. The CT parameters at both institutions were a tube voltage of 120kV, tube current of 120mA, and slice thickness of 2.0mm. Positron emission tomography scans were performed in 3D mode, from the skull vertex to the proximal thigh. Each scan took 2 minutes per bed position, with CT data used for attenuation correction. Image reconstruction utilized the ordered subset expectation maximization (OSEM) method with 3 iterations and 10 subsets on the Veros device, while the GEMINI GX used LOR (Line of Response) reconstruction.

Follow-up

All enrolled patients were followed up at 3- to 6-month intervals after treatment initiation, with the endpoint defined as overall survival (OS). The median OS for patients with cervical cancer from the two institutions was 24 months. Based on this, patients were categorized into short OS and long OS groups.

Data standardization and VOI delineation

The workflow of radiomics in this study is illustrated in Figure 2. Two nuclear medicine physicians with five years of PET/CT diagnostic experience, blinded to the patients' survival times, delineated the volumes of interest (VOI) in PET images using LIFEx software (version 7.4, http://www.lifexsoft.org; Orsay, France). The VOI included both the tumor and

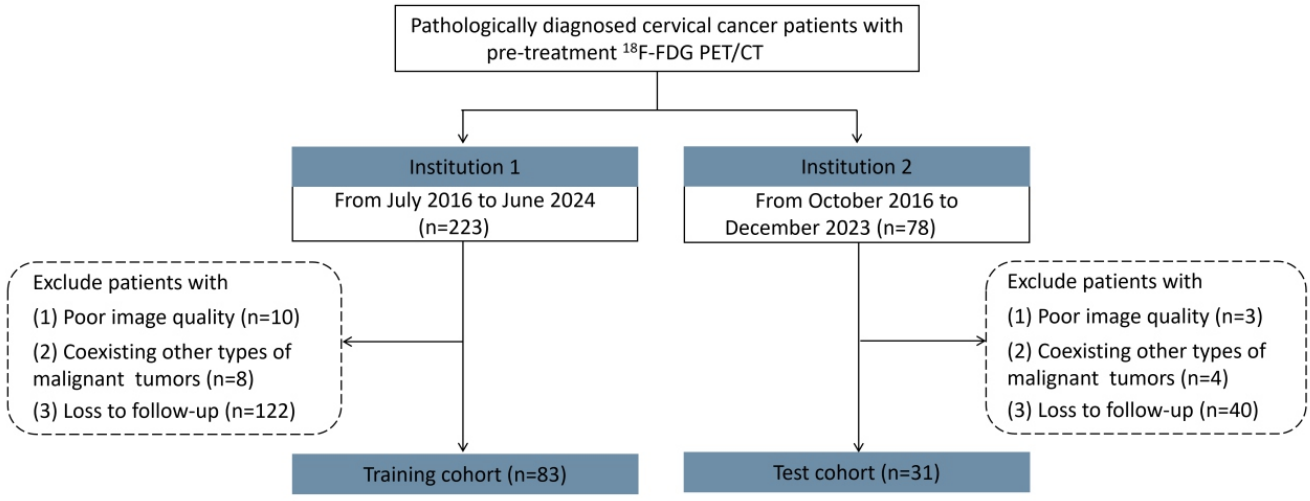

Figure 1. The enrollment of the candidates in the study was flowcharted.

peritumoral regions. To minimize discrepancies between images, the scanned images were resampled to a voxel size of 1mm×1mm×1mm. Additionally, PET images were then standardized to ensure consistent image analysis and reliable results. The standardization process involved batch-adjusting the contrast of all images to a uniform level using software, applying consistent settings across the entire dataset. The general intratumoral region, extending beyond the tumor itself, was manually delineated layer by layer. Subsequently, the intratumoral boundary was automatically defined using a standardized uptake value (SUV) threshold of 2.5. Following this, 2mm, 4mm, 6mm, and 8mm annular regions were automatically generated around the tumor boundary to delineate the peritumoral areas. Any adjacent non-tumor tissues, such as the bladder, kidneys, or surrounding normal bowel, were manually excluded from these annular regions.

Radiomics feature extraction and selection

Radiomic feature extraction was performed using the Pyradiomics module in Python 3.7.0, which extracted a total of 2016 PET-based radiomic features for each VOI. Detailed information about the extracted features is provided in Figure S1. Feature standardization was then performed using the Z-score method. To mitigate discrepancies arising from the use of different imaging devices, Combat harmonization was applied as a preprocessing step to address scanner variability.

During the radiomics feature selection process, features with a Pearson correlation coefficient exceeding 0.90 were considered highly correlated, and only the feature with higher area under the ROC curve AUC value was retained. After applying Least Absolute Shrinkage and Selection Operator (LASSO) regression, features with non-zero coefficients were selected for further analysis.

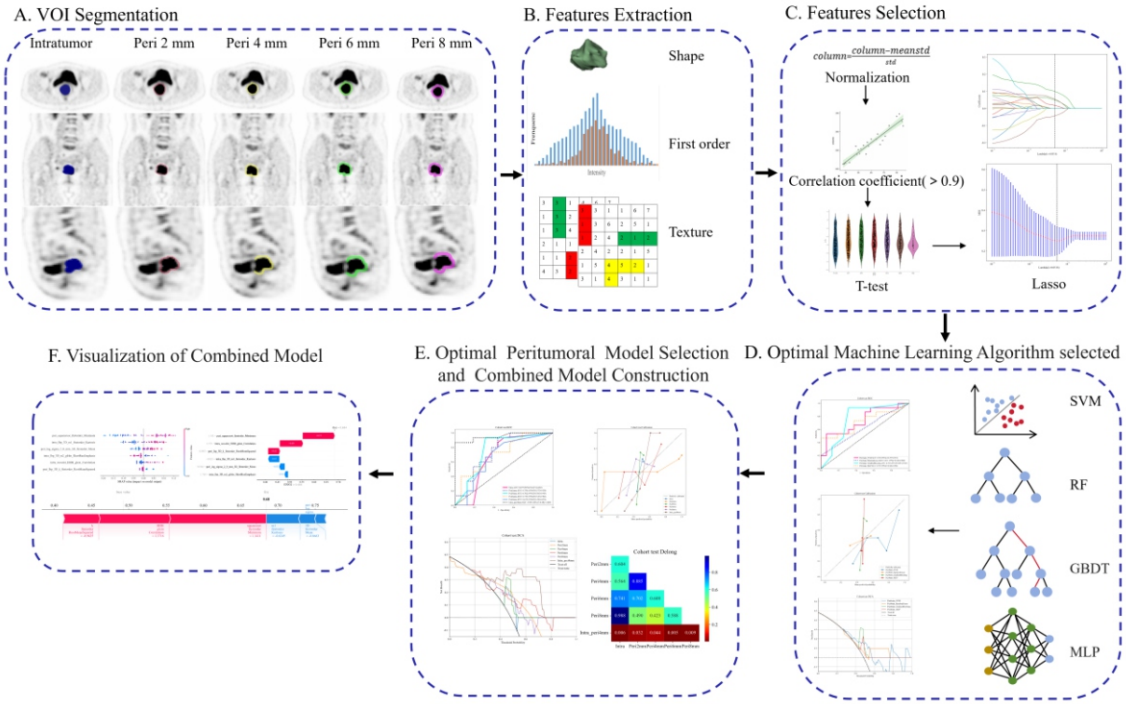

Figure 2. Flow chart of radiomics analysis.

firstorder	396
glcm	484
gldm	308
glrlm	352
glszm	352
ngtdm	110
shape	14
total	2016

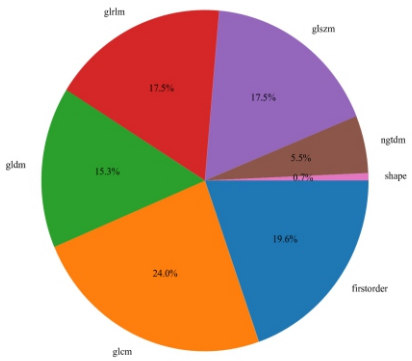

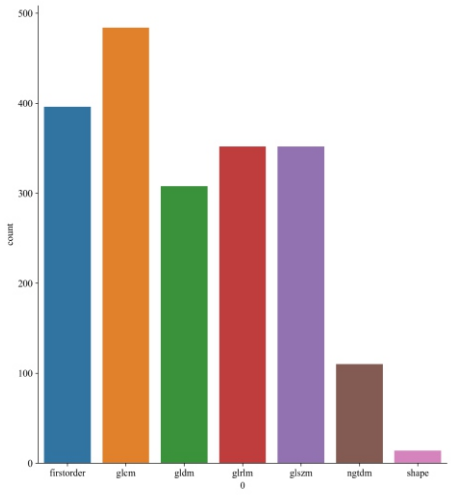

Add Figure S1 legend

Optimal machine learning algorithm selection

After radiomic feature selection, a total of 20 intratumoral and peritumoral radiomic models were constructed based on various combinations of four ensemble learning algorithms: RF, SVM, GBM, and MLP, applied across five tumor modalities (intratumoral, peritumoral 2mm, 4mm, 6mm, and 8mm). The optimal machine learning algorithm was selected from these models based on performance.

Optimal peritumoral model and combined model construction

The AUC of the optimal machine learning algorithms for the four peritumoral models were compared, and the best-performing peritumoral model was chosen. Finally, a combined model was developed by integrating the intratumoral model with the optimal peritumoral model.

Model explanation and visualization

Shapley additive explanations, a method grounded in game theory, is utilized to explain machine learning model predictions by calculating Shapley values [13]. A key advantage of SHAP is its ability to quantify the contribution of each feature to the model's prediction, ensuring consistency in the interpretation of results.

Shapley additive explanations values were used to evaluate the overall importance of features within the combined model, which demonstrated the strongest predictive performance. The SHAP summary plot visually represents the influence of each feature on the model's predictions, with each point corresponding to the SHAP value of a specific feature for an individual patient. In contrast, the SHAP force plot offers insights into the individual contributions of features to a single prediction, highlighting how variations in feature values affect the model's output. This visualization uses arrows or color coding to indicate both the direction and magnitude of positive or negative contributions, providing a transparent and intuitive explanation of the model's decision-making process.

Statistical analysis

Quantitative variables are presented as mean±standard deviation (SD), and comparisons between two independent groups were conducted using the independent-samples t-test. Categorical variables are expressed as frequencies and percentages, with comparisons made using the chi-square test or Fisher's exact test. The performance of the radiomics model was assessed using various metrics, including AUC, sensitivity, specificity, positive predictive value (PPV), and negative predictive value (NPV). Additionally, performance was evaluated through ROC curves, calibration curves, and decision curve analysis (DCA). Differences in AUC values between models were analyzed using the DeLong test. All statistical analyses were performed in Python (Anaconda3.exe), with statistical significance set at a two-sided P-value <0.05

Results

Patient characteristics

As shown in Table 1, no significant differences were observed in the clinical characteristics between the training and testing cohorts. Based on a median OS of 24 months, the cases were divided into two groups: Short OS and long OS. To identify potential clinical prognostic factors for cervical cancer, univariate logistic regression analysis was conducted. As presented in Table 2, no clinical prognostic factors were found to be independent indicators of prognosis.

Optimal machine learning algorithm based on intratumoral and peritumoral radiomics in the testing cohort

Following radiomic feature selection, a total of 5, 2, 5, 11, and 11 informative features were identified for constructing the intratumoral model (Figure S2a), peri-2mm model (Figure S2b), peri-4mm model (Figure S2c), peri-6mm model (Figure S2d), and peri-8mm model (Figure S2e), respectively. Subsequently, 20 machine learning models were developed by integrating these five radiomic models with four distinct machine learning algorithms: RF, SVM, GBM, and MLP. Among the classifiers, GBM demonstrated superior performance in prognosis prediction compared to the other three algorithms. Specifically, GBM achieved AUC values of 0.677, 0.750, 0.762, 0.719, and 0.675 for the intratumoral, peri-2mm, 4mm, 6mm, and 8mm models, respectively, in the testing cohort (Figures 3a-3f). Based on these results, GBM was selected as the optimal machine learning algorithm for further analysis.

Optimal peritumoral model selection and combined model construction

The diagnostic performance of the radiomics models using the GBM algorithm was evaluated across four different peritumoral region sizes in the testing cohort. The corresponding AUC values were 0.750, 0.762, 0.719, and 0.675, respectively. Among these models, the one incorporating a 4mm peritumoral region demonstrated superior diagnostic performance, with an optimal balance of stability and accuracy (Figure 4a).

To further enhance model performance, a combined radiomics model was developed, integrating six features that encompassed both intratumoral characteristics and those from the 4mm peritumoral region (Figure S2f). This combined model was compared against the individual intratumoral and peritumoral models. The results showed that the combined model exhibited the highest performance in the test set, achieving an AUC of 0.954, sensitivity of 0.867, specificity of 1.000, and accuracy of 0.935. The corresponding ROC curve for this optimal combined model is shown in Figure 4a. Additionally, the results of the DeLong test, which statistically compared performance differences between models, are presented in Figure 4b. The calibration curve and clinical decision analysis curve further validate the model's reliability and practical utility, as shown in Figures 4c and 4d, respectively. Finally, a comprehensive summary of the overall performance metrics for all constructed intratumoral, peritumoral, and combined models is provided in Table 3.

Visualization of combined model

Table 1. *Demographic information and clinical characteristics of patients in the training and validation cohorts.*

Characteristics	All	Training cohort	Test cohort	P value
Age#	55.55±12.79	55.55±12.72	55.55±13.18	0.998
Pathological type				0.523
squamous Cell Carcinoma	102 (89.47)	74 (89.16)	28 (90.32)	
adenocarcinoma	9 (7.89)	6 (7.23)	3 (9.68)	
others	3 (2.63)	3 (3.61)	-	
FIGO stage				0.469
I	15 (13.16)	12 (14.46)	3 (9.68)	
II	30 (26.32)	23 (27.71)	7 (22.58)	
III	49 (42.98)	32 (38.55)	17 (54.84)	
IV	20 (17.54)	16 (19.28)	4 (12.90)	
Tumor marker				0.819
normal	55 (48.25)	39 (46.99)	16 (51.61)	
elevated	59 (51.75)	44 (53.01)	15 (48.39)	
Treatment				0.642
signal	35 (30.70)	27 (32.53)	8 (25.81)	
combined	79 (69.30)	56 (67.47)	23 (74.19)	

#A t-test was used for age, a χ^2 test or Fisher's exact test was used for the rest

Table 2. *Univariate analysis in cervical cancer patients.*

	OR	OR lower 95%CI	OR upper 95%CI	P value
Age	0.998	0.992	1.005	0.634
Pathological type	0.164	0.032	0.828	0.066
FIGO stage	0.952	0.836	1.083	0.53
Tumor marker	1	0.609	1.642	1
Treatment	1	0.644	1.553	1

OR: odds ratio; CI: confidence interval

Figure 5 presents the SHAP summary plot, where each point represents the impact of a feature value on the model's prediction. Features with greater influence are ranked higher on the vertical axis, while the horizontal axis shows that positive values correlate with better prognosis, and negative values reflect poorer outcomes. Red points indicate larger feature values, while blue points correspond to smaller ones. The plot highlights that the peritumoral feature "squareroot_firstorder_Minimum" is the most significant factor in predicting cervical cancer prognosis. The distribution of this feature across the dataset reveals variability in SHAP values among patients. Notably, the color gradient indicates that an increase in the value of "Peri_squareroot_firstorder _minimum" positively contributes to the model's output, enhancing the predicted prognosis.

The SHAP force plots (Figure 6) provide a more granular explanation of individual patient predictions. These plots visually depict the SHAP values of features as forces that either increase or decrease the evaluation. Each prediction begins from the baseline value of 0.49, representing the average SHAP value across all predictions. The arrow lengths correspond to the magnitude of each feature's contribution

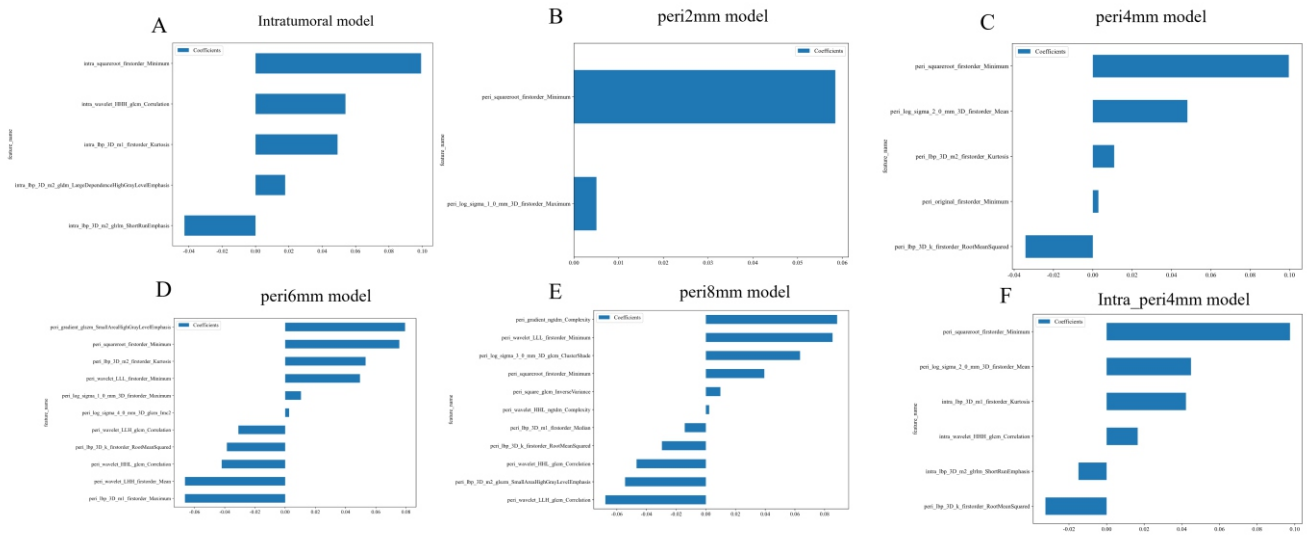

Add Figure S2 legend .

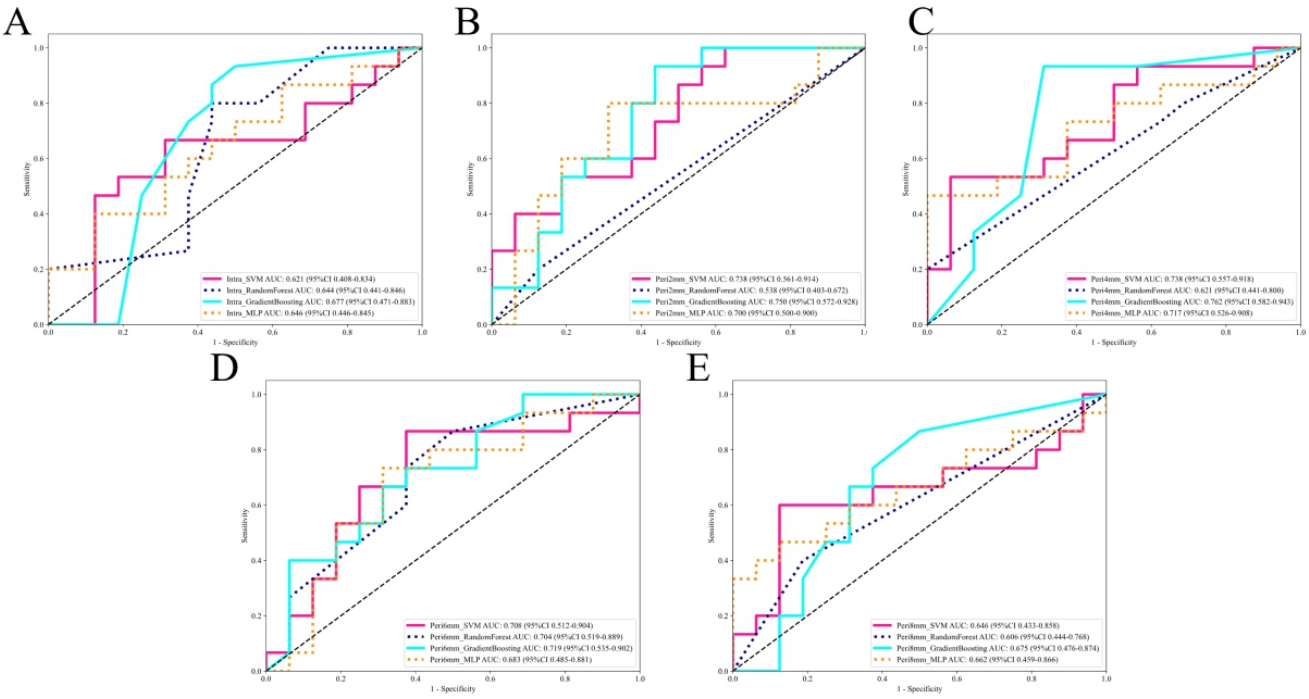

Figure 3. The ROC curves of the different models for four different algorithms in the test cohort. As indicated, Gradient Boosting was identified to be the optimal classifier with the highest AUC of 0.677, 0.750, 0.762, 0.719, and 0.675 for intratumoral (intra), peritumoral 2mm (peri2mm), peritumoral 4mm (peri4mm), peritumoral 6mm (peri6mm) and peritumoral 8mm (peri8mm) models, respectively.

to the SHAP value, expressed as a percentage. As illustrated in Figure 6A, a specific patient had a SHAP value of 0.68, surpassing the baseline value of 0.49, indicating classification into the long OS group. Among the contributing features, the red arrow for "squareroot_firstorder_Minimum" with a value of 1.141 played a pivotal role in predicting a favorable prognosis. In contrast, Figure 6B shows another patient with a SHAP value of 0.27, below the baseline value of 0.49, suggesting classification into the short OS group. The blue arrow for "squareroot_firstorder_Minimum" with a value of -1.215 reflects its negative influence on prognosis prediction, contributing to the unfavorable outcome.

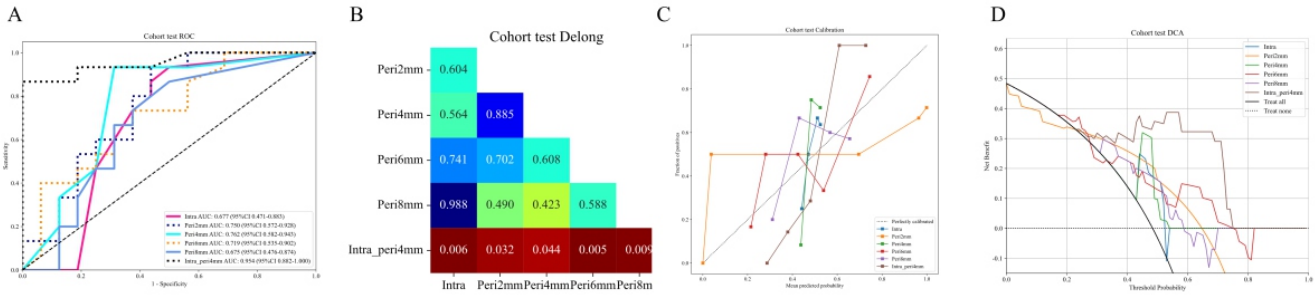

Figure 4. The performance of the intratumoral radiomic models, peritumoral radiomic models and the integrated intratumoral and peritumoral radiomic models. A) Based on PET radiomics combined with Gradient Boosting, six models were constructed: one intratumoral model (Intra), four peritumoral models (Peri2-8mm), and one intra-tumoral + peritumoral 4mm (Intra_peri4 mm) combined model. As shown in the figure, the Intra_peri4mm combined model achieved the highest average AUC of 0.954 (95% CI: 0.82–1.000) in the test cohort, proving to be the optimal model for predicting the prognosis of cervical cancer. B) The differences in prediction performance among the six constructed models are shown. C) As indicated in the calibration curves, the combined model (Intra_peri4mm) exhibited a superiority on the alignment of predicted probability and actual probability. D) The DCA curves also confirmed the outperformance of the combined model over the other models in the net benefit.

Table 3. *Each evaluation metric of the intratumoral and peritumoral models in the Gradient Boosting machine learning algorithm for the test cohort.*

Model Name	AUC (95%CI)	Accuracy	Sensitivity	Specificity	PPV	NPV	Recall	F1
Intratumoral model	0.677 (0.471 - 0.883)	0.710	0.933	0.500	0.636	0.889	0.933	0.757
Peri2mm model	0.750 (0.572 - 0.929)	0.742	0.933	0.562	0.667	0.900	0.933	0.778
Peri4mm model	0.762(0.582 - 0.944)	0.806	0.933	0.687	0.737	0.917	0.933	0.824
Peri6mm model	0.719 (0.535 - 0.902)	0.677	0.733	0.625	0.647	0.714	0.733	0.687
Peri8mm model	0.675 (0.476 - 0.874)	0.677	0.867	0.500	0.619	0.800	0.867	0.722
Combined model	0.954 (0.882 - 1.000)	0.935	0.867	1.000	1.000	0.889	0.867	0.929

AUC: area under the curve; CI: confidence interval; PPV: positive predictive value; NPV: negative predictive value; Peri2mm, peritumoral 2mm model; Peri4mm, peritumoral 4mm model; Peri6mm, peritumoral 6mm model; Peri8mm, peritumoral 8mm model.

Discussion

This study highlights the potential of integrating intratumoral and peritumoral radiomic features derived from ^{18}F-FDG PET images to predict cervical cancer prognosis. The findings emphasize the pivotal role of peritumoral imaging features, especially those from the 4 mm surrounding regions, in prognosis prediction. When combined with intratumoral features to construct a comprehensive predictive model, these features significantly enhance prediction accuracy. Furthermore, the application of SHAP values provides valuable insights into how individual and collective features contribute to prognosis prediction, thereby improving both model interpretability and clinical utility.

The peritumoral region, where tumour cells interact with adjacent normal tissue cells, represents the external tumor microenvironment [14]. Tumor invasion into surrounding

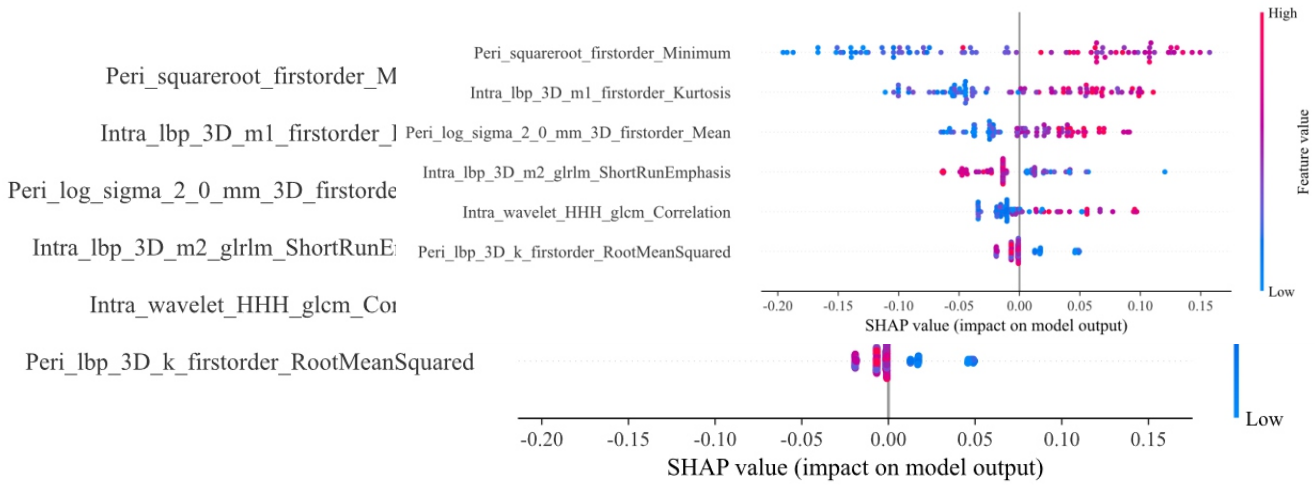

Figure 5. Shapley additive explanations summary plots of combined radiomic model (intratumoral + peritumoral 4mm model). The plot illustrated the feature relevance attributions to the model's predictive performance.

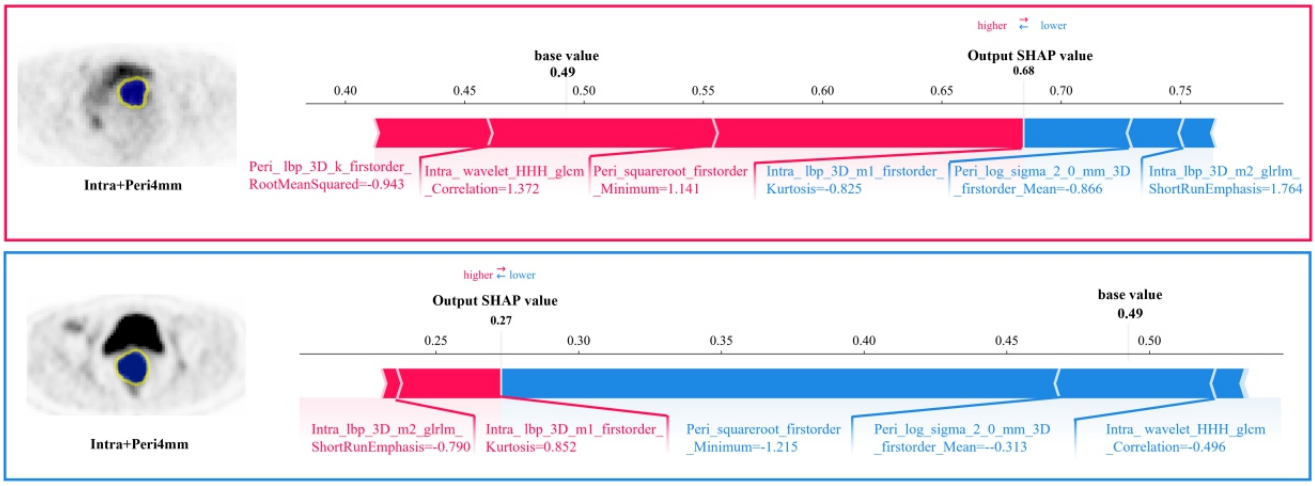

Figure 6. Shapley additive explanations force plots explained impact process of each significant features on the final predicted probability. The colour represents the contributions of each feature, with red being positive and blue being negative. The length of the colour bar represents the contribution strength. The OS of patient A was 76 months (long OS group), and the OS of patient B was 16 months (short OS group). For instance, high feature value of Peri_squareroot_firstorder_Minimum contributed to the increase in the assessment probability of the long OS group. Patient B had a Peri_squareroot_firstorder_Minimum value of -1.215, while a higher Peri_squareroot_firstorder_Minimum value of patient A (1.141) contributed to assessing the long OS group.

normal tissue can cause morphological and textural changes in the peritumoral area [15]. Radiomic features effectively capture subtle structural alterations within both tumor and peritumoral tissues, reflecting changes in the tumor microenvironment [16, 17]. Given the close association between the tumor microenvironment and tumor aggressiveness as well as treatment response, it significantly influences disease prognosis [18-21]. However, research on peritumoral radiomics in cervical cancer remains limited. Li et al. (2021) [7] explored PET/CT-based radiomics in early-stage cervical cancer, focusing on intratumoral and 2-3 mm peritumoral regions, and found that their model effectively predicted E-cadherin expression, significantly correlating with pelvic lymph node metastasis. In a study of 247 patients with early-stage cervical cancer, Zhang et al. (2023) [22] developed a radiomics model incorporating T2WI, DWI, and 3mm peritumoral regions, achieving an AUC of 0.846 for predicting lymph node metastasis. Takada et al. (2020) [23], analyzing data from 87 patients with cervical cancer, showed that features from expanded tumor regions in T2-weighted imaging (T2WI) and apparent diffusion coefficient (ADC) maps accurately predicted recurrence after radiotherapy, with AUC-ROC values of 0.82, 0.82, and 0.86 for different expanded peritumoral regions: 4mm in T2WI and 4mm and 8mm in ADC. Despite these advancements, controversy remains regarding the optimal tumor region size. This study constructed radiomics models for the peritumoral area using different thicknesses (2mm, 4mm, 6mm, and 8mm), the results show that the tumor surrounding model with a 4mm surrounding region yielded the highest predictive performance. However, as the surrounding tumor region expanded, no improvement in prediction performance was observed. This finding aligns with recent studies [24, 25], which suggest that the closer the surrounding tumor region is to the tumor inte-

rior, the richer the tumor heterogeneity information it contains. On the other hand, overly expanding the surrounding tumor region may introduce additional noise, leading to a decline in the model's predictive performance. In addition to analyzing intratumoral and peritumoral radiomics independently, a combined model integrating both intratumoral and peritumoral features were developed. The results revealed that the predictive performance of models based solely on intratumoral or peritumoral radiomics (2-8mm) was slightly lower. However, the combined model, incorporating both intratumoral and 4mm peritumoral features, significantly improved predictive accuracy. This suggests that both the internal tumor region and the 4mm peritumoral microenvironment provide valuable and complementary prognostic information.

To improve the interpretability and transparency of machine learning models, SHAP values were applied to a combined model utilizing the GBM algorithm, enhancing its explainability and evaluating the impact of key features. The use of SHAP values in cervical cancer has been explored in areas such as diagnosis [26], microbial pathogenesis [27], prediction of radiation-induced rectal inflammation post-radiotherapy [28, 29], PD-L1 and PD-1 expression prediction[30], and prognosis prediction [31]. Shapley additive explanations values assess the contribution of each feature to the model's output, and SHAP decision plots further visualize the decision-making process of the GBM algorithm. In this study, key features identified for predicting cervical cancer prognosis included the intratumoral feature lbp_3D_m1_firstorder_Kurtosis, the peritumoral feature squareroot_firstorder_Minimum, and wavelet.HHH_glcm_Correlation. The high value of lbp_3D_m1_firstorder_Kurtosis likely corresponds to regions of irregular cell growth within the tumor, represented as abnormal high- and low-density areas in imaging, suggesting increased tumor heterogeneity. Tumor heterogeneity typically reflects irregular cell growth, which is associated with tumor aggressiveness and malignancy, making it a critical prognostic factor [32]. Meanwhile, the peritumoral feature squareroot_firstorder_Minimum focuses on changes in the tumor's surrounding microenvironment. This minimum value captures alterations in the vasculature and interstitial spaces of tissue surrounding the tumor, which are essential factors influencing tumor spread and patient survival [33]. Additionally, wavelet transform analyzes image signals at various frequency scales, effectively capturing subtle but crucial texture information that may be overlooked by visual inspection. Previous studies have also shown that wavelet features possess strong predictive capabilities and play a crucial role in the construction of radiomics models [34, 35]. This study further confirms these findings. The intratumoral feature wavelet.HHH_glcm_Correlation is significantly associated with cervical cancer prognosis, suggesting that these features are robust predictors of outcomes.

This study demonstrates that the GBM algorithm, whether applied to intratumoral or peritumoral radiomic features, serves as the optimal classifier for predicting cervical cancer prognosis, showcasing its robustness. GBM excels in capturing complex nonlinear relationships and feature interactions within data [36, 37]. Ji et al. (2022) [38] successfully used the GBM algorithm to predict cancer-specific survival (CSS) in 1050 patients with intrahepatic cholangiocarcinoma using common clinical parameters, achieving a C-statistic $\geq$0.72 and outperforming traditional prognostic scoring or staging systems. Similarly, Zhao et al. (2022) [39] predicted physical therapy outcomes in 142 patients with lumbar disc herniation, with the GBM algorithm yielding the best predictive performance (AUC=0.936), outperforming the RF model (AUC=0.883). These studies suggest that the GBM algorithm is a powerful tool for both large and small sample datasets. The strong performance of the GBM algorithm in this study can be attributed to several factors. First, the iterative boosting of multiple weak learners (typically decision trees) gives GBM a high fitting ability, enabling it to handle complex nonlinear relationships and providing high predictive accuracy. Second, the study included a large number of features, particularly in the combined model with 4,032 features. As a tree-based algorithm, GBM is well-suited to handle vast feature sets and automatically select the most important ones, effectively managing high-dimensional data.

This study has several limitations. First, the sample size is relatively small, and future research could improve the generalizability of the model by incorporating a larger and more diverse patient population. Second, as this study was retrospective, certain biases may have been introduced, particularly concerning image acquisition and patient selection. Therefore, future studies should adopt standardized imaging protocols within prospective designs to further refine and validate the model. Third, this study used two different PET scanner models with consistent scanning parameters. However, the differences in reconstruction methods (OSEM and LOR) were not fully addressed as a potential limitation. These methods can impact SUV distribution and peritumoral texture features, potentially leading to variations in results. Future studies should consider standardizing reconstruction algorithms or further assess their impact on imaging features to reduce errors and biases. Additionally, integrating additional imaging modalities, such as MRI or CT, with radiomic data from PET images could provide complementary analysis to optimize model performance.

In conclusion, the radiomics of the 4-mm peritumoral region plays a pivotal role in predicting survival outcomes in cervical cancer. Furthermore, the combined radiomics model, which integrates both peritumoral and intratumoral features, has been identified as the optimal model. By integrating the GBM algorithm with SHAP value-based interpretability analysis, this study provides a robust and clinically meaningful framework for personalized prognosis prediction.

Bibliography

1. Bray F, Laversanne M, Sung H et al. Global cancer statistics 2022: GLOBOCAN estimates of incidence and mortality worldwide for 36 cancers in 185 countries. *CA A Cancer J Clinicians* 2024; 74: 229-63.
2. He B, Chen W, Liu L et al. Prediction models for prognosis of cervical cancer: Systematic review and critical appraisal. *Front Public Health* 2021; 9: 654454.
3. Cibula D, Rosaria Raspollini M, Planchamp F et al. ESGO/ESTRO/ESP guidelines for the management of patients with cervical cancer-update 2023. *Radiother Oncol* 2023; 184: 109682.

4. Espenel S, Garcia M-A, Trone J-C et al. From IB2 to IIIB locally advanced cervical cancers: Report of a ten-year experience. *Radiat Oncol* 2018; 13: 16.
5. Kucuker KA, Aksu A, Alacacioglu A, Turgut B. ^{18}Fluorodeoxyglucose positron emission tomography (18F-FDG PET)-derived tumoral and peritumoral radiomic parameters can predict pathological subtype and survival in esophageal carcinoma. *Clin Radiol* 2025; 80: 106730.
6. Zhang D, Zheng B, Xu L et al. A radiomics-boosted deep-learning for risk assessment of synchronous peritoneal metastasis in colorectal cancer. Ins*ights Imaging* 2024; 15: 150.
7. Li X, Jin J, Yu Y et al. PET-CT radiomics by integrating primary tumor and peritumoral areas predicts E-cadherin expression and correlates with pelvic lymph node metastasis in early-stage cervical cancer. *Eur Radiol* 2021; 31: 5967-79.
8. Sui C, Chen K, Ding E et al. ^{18}F-FDG PET/CT-based intratumoral and peritumoral radiomics combining ensemble learning for prognosis prediction in hepatocellular carcinoma: a multi-center study. *BMC Cancer* 2025; 25: 300.
9. Ai Y, Zhu X, Zhang Y et al. MRI radiomics nomogram integrating postoperative adjuvant treatments in recurrence risk prediction for patients with early-stage cervical cancer. *Radiother Oncol* 2024; 197: 110328.
10. Liu S, Li R, Liu Q et al. Radiomics model of ^{18}F-FDG PET/CT imaging for predicting disease-free survival of early-stage uterine cervical squamous cancer. *Cancer Biomark* 2022; 33: 249-59.
11. Yusufaly TI, Zou J, Nelson TJ et al. Improved prognosis of treatment failure in cervical cancer with nontumor PET/CT radiomics. *J Nucl Med* 2022; 63: 1087-93.
12. Najjar R. Redefining radiology: A review of artificial intelligence integration in medical imaging. *Diagnostics (Basel)* 2023; 13: 2760.
13. Nioche C, Orlhac F, Boughdad S et al. LIFEx: A freeware for radiomic feature calculation in multimodality imaging to accelerate advances in the characterization of tumor heterogeneity. *Cancer Res* 2018; 78: 4786-9.
14. Rodríguez-Pérez R, Bajorath J. Interpretation of Compound Activity Predictions from Complex Machine Learning Models Using Local Approximations and Shapley Values. *J Med Chem* 2020; 63: 8761-77.
15. Li Y, Ammari S, Lawrance L et al. Radiomics-based method for predicting the glioma subtype as defined by tumor grade, IDH mutation, and 1p/19q codeletion. *Cancers (Basel)* 2022; 14: 1778.
16. Chen S, Feng S, Wei J et al. Pretreatment prediction of immunoscore in hepatocellular cancer: A radiomics-based clinical model based on gd-EOB-DTPA-enhanced MRI imaging. *Eur Radiol* 2019; 29: 4177-87.
17. Yu Y, He Z, Ouyang J et al. Magnetic resonance imaging radiomics predicts preoperative axillary lymph node metastasis to support surgical decisions and is associated with tumor microenvironment in invasive breast cancer: A machine learning, multicenter study. *EBioMedicine* 2021; 69: 103460.
18. Wang X, Xie T, Luo J, Zhou. Radiomics predicts the prognosis of patients with locally advanced breast cancer by reflecting the heterogeneity of tumor cells and the tumor microenvironment. *Breast Cancer Res* 2022; 24: 20.
19. Sun Z, Zhang T, Ahmad MU et al. Comprehensive assessment of immune context and immunotherapy response via noninvasive imaging in gastric cancer. *J Clin Invest* 2024; 134: e175834.
20. Chen Y, Deng X, Li Y et al. Comprehensive molecular classification predicted microenvironment profiles and therapy response for HCC. *Hepatology* 2024; 80: 536-51.
21. Huang W, Jiang Y, Xiong W et al. Noninvasive imaging of the tumor immune microenvironment correlates with response to immunotherapy in gastric cancer. *Nat Commun* 2022; 13: 5095.
22. Jin M-Z, Jin W-L. The updated landscape of tumor microenvironment and drug repurposing. *Signal Transduct Target Ther* 2020; 5: 166.
23. Zhang Z, Wan X, Lei X et al. Intra- and peri-tumoral MRI radiomics features for preoperative lymph node metastasis prediction in early-stage cervical cancer. *Insights Imaging* 2023; 14: 65.
24. Takada A, Yokota H, Watanabe Nemoto M et al. A multi-scanner study of MRI radiomics in uterine cervical cancer: prediction of in-field tumor control after definitive radiotherapy based on a machine learning method including peritumoral regions. *Jpn J Radio* 2020; 38: 265-73.
25. Sui C, Chen K, Ding E et al. ^{18}F-FDG PET/CT-based intratumoral and peritumoral radiomics combining ensemble learning for prognosis prediction in hepatocellular carcinoma: a multi-center study. *BMC Cancer* 2025; 25: 300.
26. Sui C, Su Q, Chen K et al. ^{18}F-FDG PET/CT-based habitat radiomics combining stacking ensemble learning for predicting prognosis in hepatocellular carcinoma: A multi-center study. *BMC Cancer* 2024; 24: 1457.
27. Yang X, Gao C, Sun N. An interpretable clinical ultrasound-radiomics combined model for diagnosis of stage I cervical cancer. *Front Oncol* 2024; 14: 1353780.
28. Sekaran K, Varghese RP, Gopikrishnan M et al. Unraveling the dysbiosis of vaginal microbiome to understand cervical cancer disease etiology-an explainable AI approach. *Genes (Basel)* 2023; 14: 936.
29. Xue J, Wu M, Zhang J et al. Delta-radiomics analysis based on magnetic resonance imaging to identify radiation proctitis in patients with cervical cancer after radiotherapy. *Front Oncol* 2025; 15: 1523567.
30. Wei C, Xiang X, Zhou X et al. Development and validation of an interpretable radiomic nomogram for severe radiation proctitis prediction in postoperative cervical cancer patients. *Front Microbiol* 2022; 13: 1090770.
31. Liu KH, Yang W, Tian HP. Relationships between intravoxel incoherent motion parameters and expressions of programmed cell death-1 (PD-1) and programmed cell death ligand-1 (PD-L1) in patients with cervical cancer. *Clin Radiol* 2024; 79: e264-72.
32. Wang Y, Yu Y, Gu L et al. Radiomics feature is a risk factor for locally advanced cervical cancer treated using concurrent chemoradiotherapy based on magnetic resonance imaging: A retrospective study. *BMC Cancer* 2025; 25: 230.
33. Xie Y, Wang M, Xia H et al. Development and validation of a CECT-based radiomics model for predicting IL1B expression and prognosis of head and neck squamous cell carcinoma. *Front Oncol* 2023; 13: 1121485.
34. Ouyang Q, Chen Q, Zhang L et al. Construction of a risk prediction model for axillary lymph node metastasis in breast cancer based on gray-scale ultrasound and clinical pathological features. *Front Oncol* 2024; 14: 1415584.
35. Wang X, Zhao X, Li Q et al. Can peritumoral radiomics increase the efficiency of the prediction for lymph node metastasis in clinical stage T1 lung adenocarcinoma on CT? *Eur Radiol* 2019; 29: 6049-58.
36. Wang Y, Zhao H, Fu P et al. Preoperative prediction of lymph node metastasis in colorectal cancer using 18F-FDG PET/CT peritumoral radiomics analysis. *Med Phys* 2024; 51: 5214-25.
37. Zhang Z, Zhao Y, Canes A et al. written on behalf of AME Big-Data Clinical Trial Collaborative Group. Predictive analytics with gradient boosting in clinical medicine. *Ann Transl Med* 2019; 7: 152.
38. Cai F, Guo Z, Wang G et al. Integration of intratumoral and peritumoral CT radiomic features with machine learning algorithms for predicting induction therapy response in locally advanced non-small cell lung cancer. *BMC Cancer* 2025; 25: 461.
39. Ji G-W, Jiao C-Y, Xu Z-G et al. Development and validation of a gradient boosting machine to predict prognosis after liver resection for intrahepatic cholangiocarcinoma. *BMC Cancer* 2022; 22: 258.
40. Zhao P, Xue J, Xu X et al. Logistic model and gradient boosting machine model for physical therapy of lumbar disc herniation. *Comput Math Methods Med* 2022: 4799248.